# Defining the Kv2.1–syntaxin molecular interaction identifies a first-in-class small molecule neuroprotectant

Chung-Yang Yeh[a,b,1], Zhaofeng Ye[c,d,1], Aubin Moutal[e], Shivani Gaur[a,b], Amanda M. Henton[f,g], Stylianos Kouvaros[f,g], Jami L. Saloman[a], Karen A. Hartnett-Scott[a,b], Thanos Tzounopoulos[a,f,g], Rajesh Khanna[e], Elias Aizenman[a,b,g,2], and Carlos J. Camacho[c,2]

[a]Department of Neurobiology, University of Pittsburgh School of Medicine, Pittsburgh, PA 15261; [b]Pittsburgh Institute for Neurodegenerative Diseases, University of Pittsburgh School of Medicine, Pittsburgh, PA 15261; [c]Department of Computational and Systems Biology, University of Pittsburgh School of Medicine, Pittsburgh, PA 15261; [d]School of Medicine, Tsinghua University, Beijing 100871, China; [e]Department of Pharmacology, College of Medicine, University of Arizona, Tucson, AZ 85724; [f]Department of Otolaryngology, University of Pittsburgh School of Medicine, Pittsburgh, PA 15261; and [g]Pittsburgh Hearing Research Center, University of Pittsburgh School of Medicine, Pittsburgh, PA 15261

Edited by Lily Yeh Jan, University of California, San Francisco, CA, and approved June 19, 2019 (received for review February 27, 2019)

**The neuronal cell death-promoting loss of cytoplasmic $K^+$ following injury is mediated by an increase in Kv2.1 potassium channels in the plasma membrane. This phenomenon relies on Kv2.1 binding to syntaxin 1A via 9 amino acids within the channel intrinsically disordered C terminus. Preventing this interaction with a cell and blood-brain barrier-permeant peptide is neuroprotective in an in vivo stroke model. Here a rational approach was applied to define the key molecular interactions between syntaxin and Kv2.1, some of which are shared with mammalian uncoordinated-18 (munc18). Armed with this information, we found a small molecule Kv2.1–syntaxin-binding inhibitor (cpd5) that improves cortical neuron survival by suppressing SNARE-dependent enhancement of Kv2.1-mediated currents following excitotoxic injury. We validated that cpd5 selectively displaces Kv2.1–syntaxin-binding peptides from syntaxin and, at higher concentrations, munc18, but without affecting either synaptic or neuronal intrinsic properties in brain tissue slices at neuroprotective concentrations. Collectively, our findings provide insight into the role of syntaxin in neuronal cell death and validate an important target for neuroprotection.**

Kv2.1 | syntaxin | neurodegeneration | neuroprotection

Therapeutic options to prevent, halt, or ameliorate neurodegenerative disorders remain critical areas of unmet medical need despite more than 3 decades of aggressive research efforts (1, 2). Central to this challenge is the fact that many neurologic diseases are driven by proteins with highly flexible and unstructured domains that bind multiple partners, making both their mechanistic characterization and their pharmacologic targeting exceedingly difficult (3). Indeed, these intrinsically disordered unstructured domains are quite common among various disease-associated membrane-bound receptors and ion channels, especially in their regulatory cytoplasmic regions (4). One such protein is the delayed rectifier potassium channel Kv2.1, which enables a well-characterized neuronal cell death cascade through its cytoplasmic C terminus domain (5). In the present study, we focused on a key interactor of the Kv2.1 C terminus, syntaxin 1A (syntaxin), to further unveil the molecular mechanisms involved in Kv2.1-dependent neurodegeneration and to pursue a novel translational strategy.

Following an injurious stimulus, Kv2.1-mediated regulation of intracellular $K^+$ is a critical convergent factor in neuronal cell death programs. At normal physiological concentrations, cytoplasmic $K^+$ suppresses the catalytic activity of several proteases and nucleases linked to cellular pathology (6); however, enhanced $K^+$ efflux in injured neurons facilitates rapid execution of cell death cascades (7, 8). Kv2.1 mediates this cell death-promoting cytoplasmic $K^+$ loss in a number of neuronal subtypes, including cortical neurons (9), hippocampal pyramidal neurons (10, 11), midbrain dopaminergic neurons (12), and cerebellar granule cells (13). The Kv2.1-dependent cell death pathway is normally initiated by the oxidative liberation of zinc from intracellular metal-binding proteins (14), leading to the sequential phosphorylation of Kv2.1 residues Y124 and S800 by Src and p38 kinases, respectively (15–17). The dual phosphorylation of the channel enhances its interaction with syntaxin and increases its surface expression, inducing the subsequent loss of intracellular $K^+$ (5, 9, 12, 18, 19).

The Kv2.1 domain responsible for the interaction with syntaxin is located within the intrinsically disordered Kv2.1 proximal cytosolic C-terminal, originally termed C1a (20–22). Overexpression of a fragment containing residues 441–522 within the C1a region (Kv2.1 rat sequence; GenBank accession no. NP_037318.1) is sufficient to inhibit the injury-induced plasma membrane insertion of Kv2.1 channels in neurons and provide neuroprotection in vitro (23). Recently, we further narrowed down the amino acid sequence within C1a to 9 residues: $H_1$LSPNKWKW$_9$ (C1aB; from N to C terminus, corresponding to Kv2.1 residues 478–486 in rat and 482–490 in mouse and humans; accession nos. NP_032446.2 and NP_004966.1, respectively). Most importantly, blocking the interaction between Kv2.1 and syntaxin using a blood-brain barrier-permeable conjugated peptide (TAT-C1aB) effectively ameliorates

## Significance

**An enhanced Kv2.1–syntaxin interaction precedes the neuronal cell death-promoting loss of cytosolic $K^+$ in many neurodegenerative conditions. The work presented here characterizes the interaction of the disordered C terminus of Kv2.1 to syntaxin at a molecular level and further translates these findings to discover a first-in-class small molecule with neuroprotective properties. In doing so, we demonstrate a rational drug discovery workflow that can elucidate protein–protein interactions involving highly unstructured domains.**

Author contributions: C.-Y.Y., Z.Y., A.M., T.T., R.K., E.A., and C.J.C. designed research; C.-Y.Y., Z.Y., A.M., S.G., A.M.H., S.K., J.L.S., K.A.H.-S., and C.J.C. performed research; C.-Y.Y., Z.Y., A.M., S.G., A.M.H., S.K., J.L.S., T.T., R.K., E.A., and C.J.C. analyzed data; and C.-Y.Y., E.A., and C.J.C. wrote the paper.

Conflict of interest statement: E.A. has a patent on the use of Kv2.1-derived peptides (US Patent 9,932,382). C.J.C. and E.A. have filed a patent on the use of small molecules to disrupt Kv2.1–syntaxin interaction (Provisional Patent Application 62/712,514).

This article is a PNAS Direct Submission.



[1]C.-Y.Y. and Z.Y. contributed equally to this work.

[2]To whom correspondence may be addressed. Email: redox@pitt.edu or ccamacho@pitt.edu.

This article contains supporting information online at www.pnas.org/lookup/suppl/doi:10.1073/pnas.1903401116/-/DCSupplemental.

Published online July 15, 2019.

acute neuronal ischemic injury, limiting infarct damage and improving neurologic function in vivo (24).

The chemical disruption of protein–protein interactions involving intrinsically disordered regions such as the Kv2.1 C terminus is a unique challenge for pharmaceutical intervention, as these domains not only undergo structural rearrangements on binding, but also involve selectively promiscuous sites that regulate multiple interactions (25). This task is further hindered by the fact that the syntaxin site for Kv2.1 binding has not yet been resolved. To address these challenges, we developed a rational approach that combines molecular modeling, biophysics, and cell-based experimental validations. This approach led us to elucidate the molecular actors essential to the Kv2.1–syntaxin interaction, predicting it to exist within the complex binding site previously resolved for the cocrystal structure between syntaxin and mammalian uncoordinated 18 (munc18), a critical component in exocytotic processes (26). We then began translating these results by a virtual screening of small molecule libraries, with the goal of inhibiting the Kv2.1-syntaxin interaction while minimally interfering with munc18 function. This process led to the identification of a first-in-class protein–protein interaction inhibitor and lead compound that can prevent neuronal injury. These findings reveal mechanistic insight into syntaxin's role in cell death functions and validate a novel target for the development of neuroprotective therapeutics.

## Results

**Structural Modeling of Kv2.1 C1aB $H_1$LSPNKWKW$_9$ Peptide and Its Interactions with Syntaxin.** Syntaxin binding to the C1a region of Kv2.1 is largely restricted to within a 9-aa sequence of the channel that we previously defined as C1aB ($H_1$LSPNKWKW$_9$). We had observed a rapid dropoff in syntaxin binding when C-terminal C1aB residues were removed in a large avidity panel of Kv2.1 C1a-derived 15-mer peptides (24), alerting us to the possibility that the essential interactions of the syntaxin-binding domain could be further refined. We thus carried out molecular dynamics simulations of Kv2.1-derived peptides containing partial or complete C1aB sequences to analyze the stability of these peptides. Fig. 1 *A* and *B* show both a representative snapshot and the conformational ensembles entailed by the C1aB K6W7 sequence motif for 4 different peptides. Two of the strongest syntaxin-binding peptides (24), pep-22 and pep-28, consistently show a fully solvent-exposed W7 residue with the preceding K6 in the opposite *trans* direction. In contrast, the 2 weakest syntaxin-binding peptides, pep-20 and pep-21, show increasing occlusion of W7 by interactions with the K6 side chain on deletion of either the K8W9 residues or just the W9 from the corresponding C1aB sequence. This is evidenced by the increasing probability of K6 to be in the interfering *cis* positions when the 2 anchoring residues are removed in the weakly binding peptides (Fig. 1*B*). The observed stability of the free W7 in strongly binding peptides suggests that this residue plays a critical role in the recognition of syntaxin, whereas deletion of W9 could have an impact on binding affinity by inducing the occlusion of W7; however, as suggested by our previous work (24), the shorter peptide would still able to bind the SNARE protein to some extent.

**The Kv2.1 C1aB W7 Syntaxin-Binding Structural Motif Is Shared with munc18 W28.** The cocrystal structure of the closed form of syntaxin and munc18 (Protein Data Bank [PDB] ID code 4JEH) (26, 27), a known modulator of synaptic transmission essential for the proper assembly of syntaxin with other SNARE components (28), is stabilized by multiple hydrogen bonds and nonpolar interactions encompassing both the syntaxin regulatory Habc and core SNARE H3 domains. This includes a specificity determinant aromatic stacking between munc18 W28 and syntaxin F34 on the first helix of the Habc domain (Fig. 2*A*). Structural similarities between our simulated C1a peptides (Fig. 1*A*) and the corresponding motif in munc18 bound to syntaxin (Fig. 1*C*), which also has an adjacent lysine residue (K29), led us to perform unbiased docking of a C1aB peptide on syntaxin's binding surface with munc18. Using SMINA software (29) with default settings, we obtained the C1aB docked pose shown in Fig. 2*B*.

**Experimental Validation of C1aB–Syntaxin Interactions.** All the intermolecular interactions in our C1aB–syntaxin-binding model (detailed view in Fig. 2*D*) are not only chemically favorable, but also strikingly consistent with an alanine scan mutagenesis of individual C1aB amino acids in a syntaxin-binding peptide array assay (Fig. 1*D*). In particular, 1) W7 stacking interaction with syntaxin F34 is eliminated in W7A, but nonpolar contacts remain; 2) W9 hydrophobic contacts with syntaxin I115 are absent in W9A, thereby significantly decreasing binding affinity; 3) the C1aB K6 backbone, whose side chain is opposite to W7, interacts via hydrogen bonds with Q119, a property retained in K6A; 4) L2 is buried in a hydrophobic pocket formed by syntaxin L123, K126, and T122, and thus the hydrophobic side chain present in L2A may decrease binding affinity somewhat; and 5) C1a H1 hydrogen bonds with T122 and D231 are expected to be replaced in H1A, with D231 bonding to the free amine group in the N terminus of the peptide.

Of note, interactions equivalent to those seen in our C1aB model are also observed in the munc18 and syntaxin cocrystal (Fig. 2*C*), further supporting the accuracy of our proposed model. Specifically, and as shown in detailed contacts of munc18 and syntaxin in Fig. 2*C*, 1) munc18 W28 stacking with syntaxin F34, with the nearby K29 pointing in the opposite direction, is analogous to the arrangement of C1aB W7; 2) munc18 T56 and I57 contact syntaxin I115, analogous to the interactions of C1aB W9; 3) the crystal water in the munc18 binding interface, fully coordinated by syntaxin Q119, T122, and R41 together with the munc18 M51 backbone, is reshaped into a nonpolar pocket in syntaxin, burying C1aB L2; and 4) the munc18 T48 hydrogen bond with syntaxin D231 is mimicked by C1aB H1. Taken together, unbiased docking of C1aB peptide fully rationalizes the alanine scanning, where W7 aromatic stacking with syntaxin F34 and the burial of L2 in a nonpolar pocket are the specificity determinant interactions of Kv2.1 C1aB with syntaxin. Notably, deletion of either of these residues in our C1a-derived 15-mer peptides obliterates binding (24) (see Fig. 5).

**Virtual Screening of Kv2.1-Syntaxin Interaction Inhibitors Identifies 6 Small Molecule Candidates.** Leveraging the aforementioned structural insights, we performed a small molecule virtual screening with the goal of inhibiting C1aB protein–protein interaction with syntaxin. To do this, we designed pharmacophore models and used the search engine ZINCPharmer (30) to screen 26+ million commercially available compounds present in the ZINC database (31). The models were designed to include a ring-stacking interaction with F34 and also to match different combinations of hydrogen bonds formed by crystal water 315 in PDB 4JEH with syntaxin Q119, T122, and R41 (Fig. 2 *A* and *C*). After the primary screening based on these pharmacophores, compounds matching our design underwent an all atom optimization (32), resulting in the 6 molecules shown in Fig. 3*A* selected for in vitro experimental testing. *SI Appendix*, Fig. S1 *A* and *B* shows the chemical structures of these selected compounds, abbreviated as cpd1 to cpd6.

**Cell-Based Screening of Small Molecule cpd5 Reveals Neuroprotective Properties.** To determine whether cpd1–6 can recapitulate the previously described biological effects of C1a and TAT-C1aB (23, 24), we evaluated them in vitro first for intrinsic toxicity and then for neuroprotective actions in rat cultured cortical neurons. We found that cpd1 did not readily dissolve at a reasonable

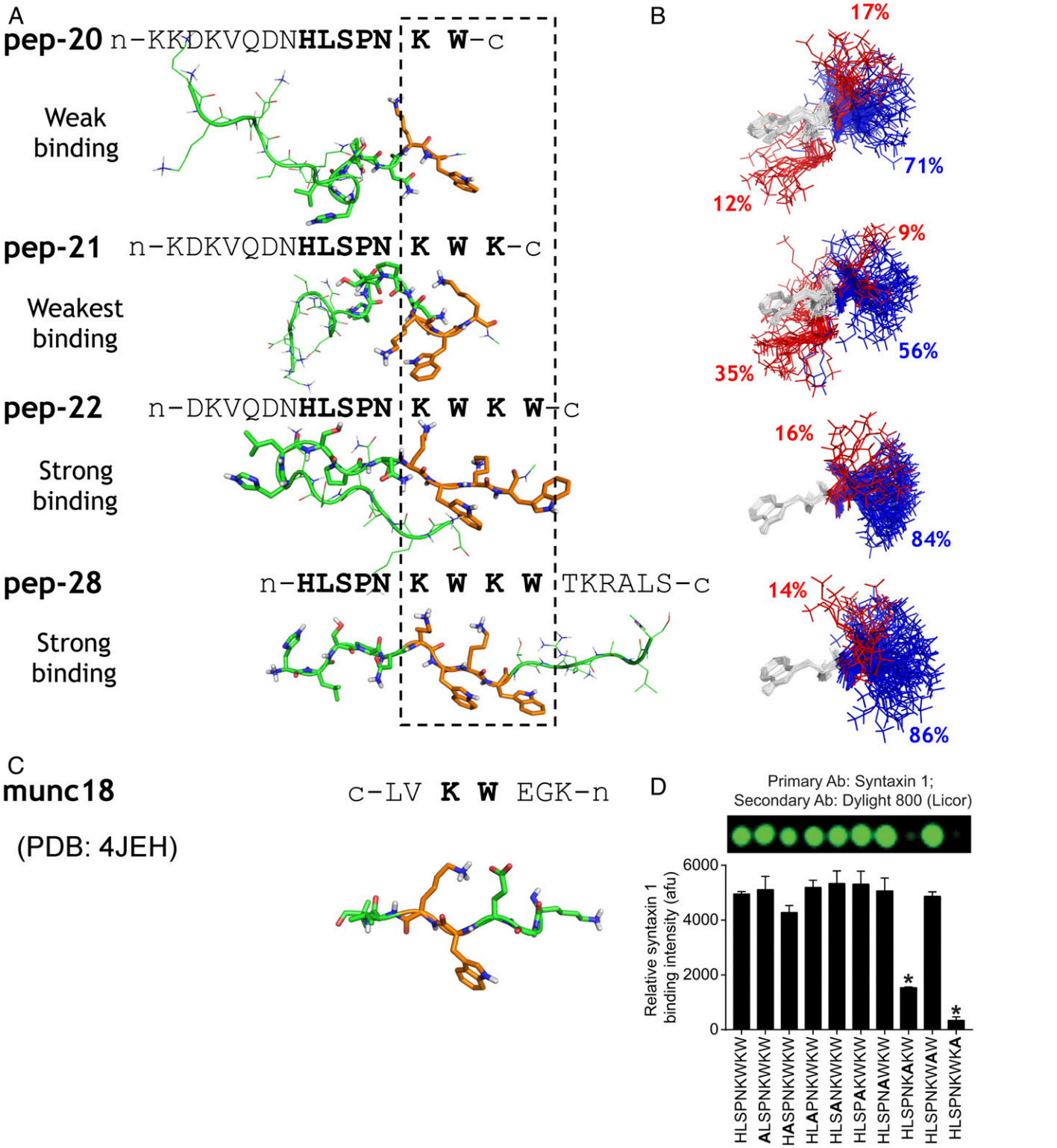


**Fig. 1.** Structural analysis and validation of Kv2.1 syntaxin-binding peptides. (*A*) Representative molecular dynamics snapshots of 4 Kv2.1-derived peptides labeled with their relative binding strength (24). From top to bottom, Kv2.1 peptide sequences containing up to W7 (pep-20), K8 (pep-21), and the entire C1aB region (pep-22, pep-28) are shown. (*B*) Assembly of 100 snapshots of K6W7 from the corresponding peptides sampled every 4 ns after 100 ns of equilibration. Snapshots were aligned on W7 (gray) with K6 sampling both possibly interfering cis (red) and noninterfering trans (blue) conformations. The W7s of the strongly binding peptides (pep-22 and pep-28) were solvent-exposed and ready to make contact with interacting surfaces. This is disrupted in pep-20 and pep-21, peptides with direct contacts between K6 and W7 side chains. (*C*) A similar structural motif as C1aB is observed in munc18 W28K29 when bound to syntaxin (PDB ID code 4JEH). (*D*) Peptide array binding assay of the C1aB sequences with sequential alanine substitutions, 1 residue at a time. Tryptophan to alanine-substituted peptides showed significantly less syntaxin binding than the parent peptide. $*P < 0.05$, ANOVA/Dunnett test. Results indicate mean ± SEM of fluorescent signal intensity in 4 independent assays.

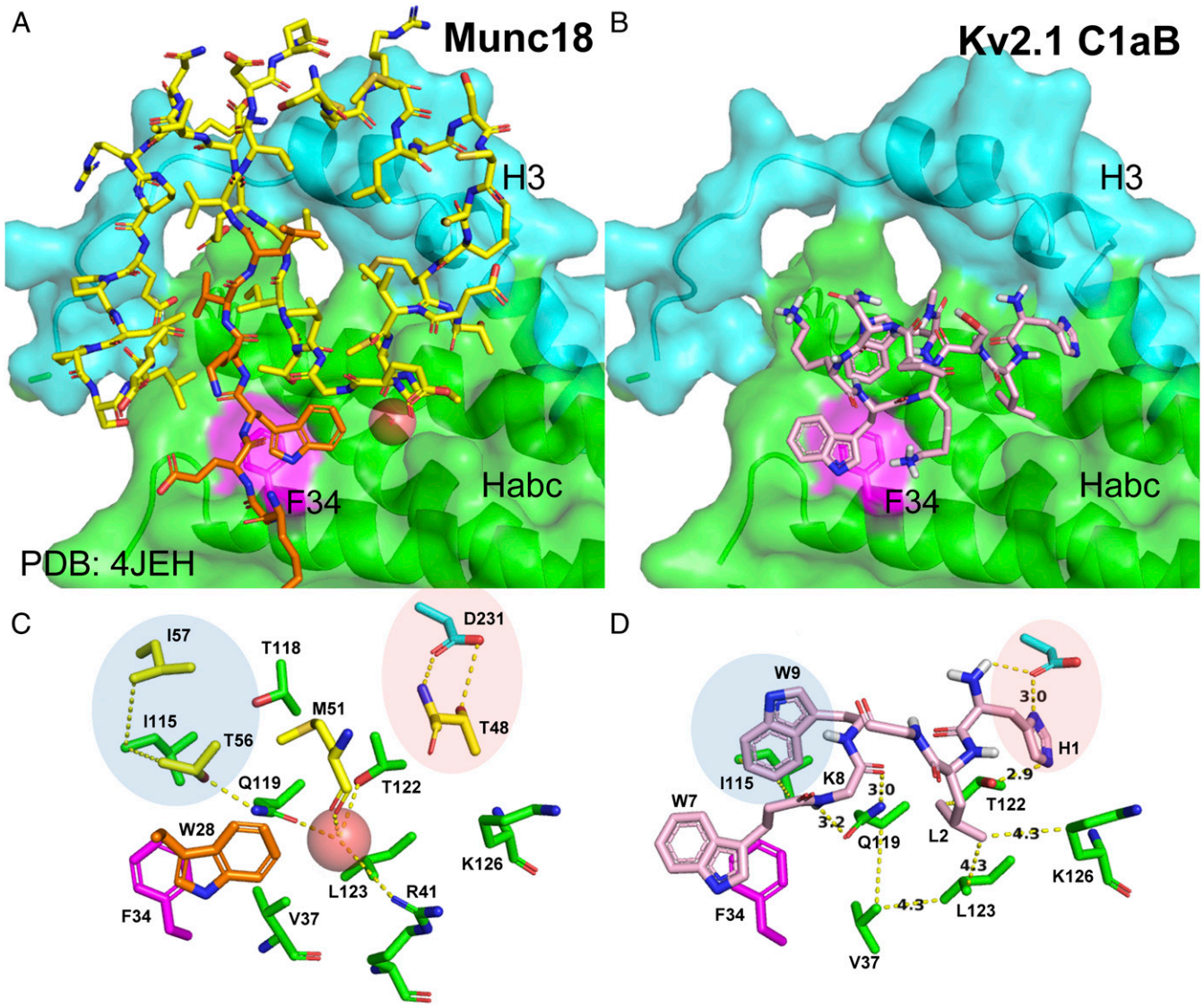


**Fig. 2.** Docked C1aB peptide recapitulates interactions of the munc18/syntaxin cocrystal. The closed form of syntaxin from munc18 cocrystal (PDB ID code 4JEH) is shown in green and cyan (surface/sticks), corresponding to the Habc and the H3 domains, respectively. Syntaxin F34 is shown in magenta to emphasize the specific aromatic stacking interaction in all panels. (*A*) Partial view of munc18/syntaxin cocrystal. Orange sticks show the same munc18 peptide as in Fig. 1*C*; other munc18 residues with favorable interactions are shown in yellow sticks. The red sphere highlights fully coordinated crystal water. (*B*) Unbiased docking model of C1aB/syntaxin. (*C* and *D*) Highlighted intermolecular interactions of munc18/syntaxin (*C*) and detailed view of interactions between the docked pose of C1aB and syntaxin (*D*). Specifically, munc18 W28 aromatic stacking is mimicked by C1aB W7, hydrophobic interactions between munc18 I57 and T56 and syntaxin I115 are mirrored by C1aB W9 (blue), and the hydrogen bond between munc18 T48 and syntaxin D231 is reproduced by H1 in C1aB (red). Syntaxin is identical in all the structures except the Q119 and T122 side chains in C1aB/syntaxin, which in the absence of the crystal water rotate slightly to satisfy its hydrogen bonds and methyl group interactions.

concentration using a variety of solvents. We also observed that cpd2 was at times neurotoxic after 24 h of incubation at 10 μM (*SI Appendix*, Fig. S1*C*), quantified as a significant increase in extracellular lactate dehydrogenase (LDH) above baseline (relative toxicity), a sign of cellular damage (33). Therefore, cp1 and cpd2 were excluded from further studies. The remaining 4 compounds were not neurotoxic at concentrations as high as 10 μM (*SI Appendix*, Fig. S1 *C* and *D*).

We next examined whether these molecules could provide neuroprotection against overnight applications of threo-β-benzyloxyaspartate (TBOA; 75 μM), a nonselective glutamate reuptake inhibitor (34). TBOA induces relatively slow (overnight) NMDA receptor-mediated excitotoxicity, characterized by Kv2.1-dependent cell death in our cultures (24, 35). We found that pretreatment for 1 h and coincubation with 10 μM cpd5 (3-[3-(1,3-benzothiazol-2-yl)phenyl]-1-[(3,4-dimethoxyphenyl)methyl]urea; MolPort-009-741-732) significantly diminished TBOA toxicity, an effect nearly identical to the actions of 1 μM TAT-C1aB treatment (Fig. 4 *A* and *B*). In phase-contrast imaging, we observed that TBOA treatment reduced the number of phase-bright, healthy neurons, which was ameliorated by cotreatment with cpd5 (Fig. 4*A*, *Left*). To better visualize this result, we transfected neurons with eGFP before treatment and confirmed that TBOA treatment caused significant cellular damage, which was ameliorated in cells cotreated with cpd5 (Fig. 4*A*, *Right*). In contrast to cpd5, cpd3, cpd4, and cpd6 did not afford any measurable neuroprotection and thus were also excluded from further analysis (*SI Appendix*, Fig. S1*E*).

The docked pose of cpd5 with syntaxin, shown in Fig. 3 *A* and *B*, recapitulates all the interactions that we found to be essential

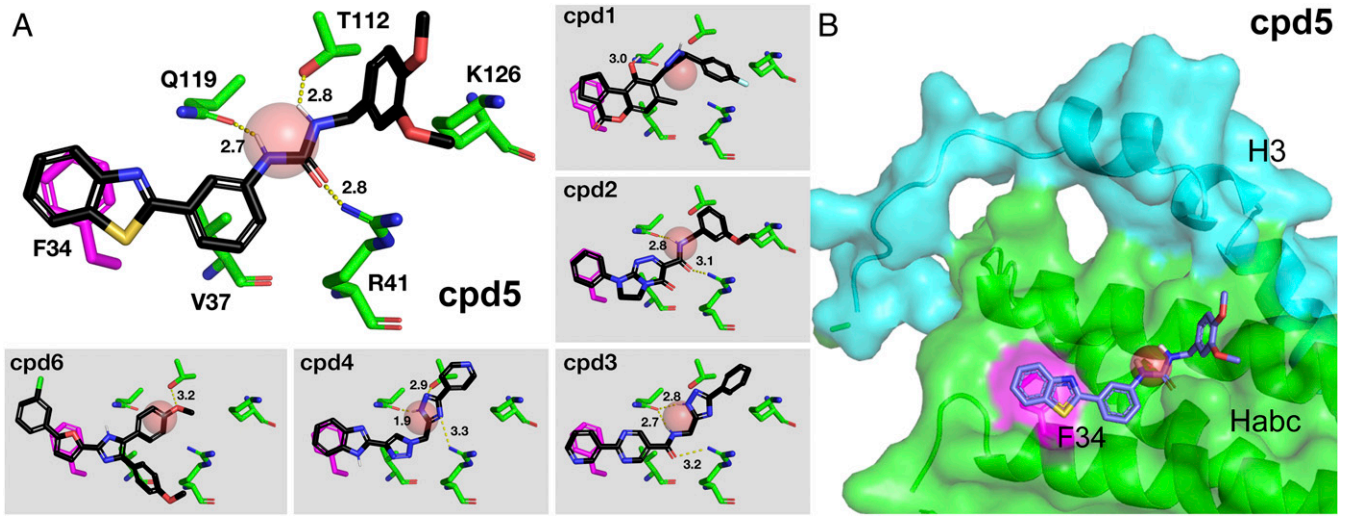


**Fig. 3.** Virtual screening discovered 6 compounds (cpd1–6) that potentially recapitulate munc18–C1aB interactions with syntaxin. (*A*) Interactions between cpd1–6 and syntaxin. For cpd5 specifically, benzothiazole ring forms a stacking interaction with F34, with urea moiety fully recapitulating hydrogen bonds formed by crystal water in munc18 (red sphere). A water molecule is shown as a guide to highlight the overlap with the urea moiety of cpd5. (*B*) Docking model of cpd5/syntaxin.

for C1aB binding to syntaxin. Namely, it shows an optimal stacking with F34 through the benzothiazole ring; hydrophobic contact between the benzene ring and V37; hydrogen bonds with A41, N119, and T122, all established by the munc18 crystal water and essential for C1aB L2 binding to syntaxin; and interaction of the veratrole group and K126. This fully supports cpd5 as potentially effective in disrupting the Kv2.1–syntaxin interaction. Mechanistically, dispersal of somatodendritic Kv2.1 clusters has also been identified as a viable approach for preventing the increase of death-inducing $K^+$ currents (36). To rule out the possibility that cpd5 is providing neuroprotection by declustering Kv2.1, we transfected neurons with Kv2.1-eGFP and evaluated their clustering status after 24 h exactly as described previously (36). We found no significant effect of 24 h of 10 μM cpd5 treatment on Kv2.1 clusters (*SI Appendix*, Fig. S1*F*). This finding is consistent with the previously observed lack of declustering properties of Kv2.1 C1a overexpression in cortical neurons (36), strongly suggesting that inhibiting the Kv2.1–syntaxin interaction subdues the translocation of new Kv2.1 channels to the membrane.

**Cpd5 Suppresses Cell Death-Enabling $K^+$ Currents.** The hallmark of Kv2.1-facilitated neuronal cell death is the accompanying large increase in delayed rectifier $K^+$ currents as the result of syntaxin-dependent de novo Kv2.1 channel insertion in the plasma membrane (19). We previously showed that plasmid-mediated overexpression of C1a or use of the TAT-C1aB peptide prevents this Kv2.1-mediated current surge (23, 24). To determine whether cpd5 achieves a similar inhibition of current enhancement, we obtained whole-cell patch clamp recordings of rat cortical neurons in vitro after coincubation with TBOA (50 μM for 2 h, followed by a 2-h wash period), a treatment previously shown to cause the canonical Kv2.1 current increase (35). In strong agreement with our neuroprotection assays, we found that cpd5 (10 μM) preloading (for 1 h) and cotreatment with TBOA effectively suppressed the postinjury enhancement of delayed rectifier $K^+$ currents in neurons to levels comparable to those in uninjured neurons (Fig. 4*C*, striped red bar). Importantly, we found no significant effects of cpd5 incubation alone on basal $K^+$ currents (Fig. 4*C*, red bar), strongly suggesting that the preexisting membrane-bound channels and the normal trafficking of the channel during the 5-h cpd5 incubation are unaffected by the drug. This is consistent with previous findings in cells expressing the C1a fragment or treated with TAT-C1aB (23, 24). Most significantly, inhibition of the injury-enhanced currents, a syntaxin-dependent process (19), strongly points to an on-target action of cpd5.

Because NMDA receptors mediate the neurotoxicity elicited by glutamate reuptake inhibitors (37), we evaluated whether cpd5 inhibits NMDA-evoked $Ca^{2+}$ response, a major component of acute excitotoxicity (38, 39). To do so, we performed Fura-2 ratiometric $Ca^{2+}$ imaging in cultured neurons during NMDA exposure (30 μM with 10 μM glycine), and noted a lack of effect of concurrently administered cpd5 (10 μM) on NMDA-evoked $Ca^{2+}$ responses (Fig. 4*D*). This strongly indicates that the aforementioned neuroprotective actions of cpd5 likely are not a result of direct interference with the upstream components of the excitotoxic cascade, but rather that cpd5, like TAT-C1aB, provides neuroprotection against TBOA-induced excitotoxicity specifically by preventing the expression of enhanced Kv2.1-mediated $K^+$ currents.

**Cpd5 Is a First-in-Class Inhibitor of Kv2.1 Binding to Syntaxin.** The docked model of cpd5 shown in Fig. 3*B* predicts that cpd5 strongly competes with essential interactions of C1aB and syntaxin. In addition, since munc18 binds to both the core SNARE domain and the N-terminal region of the closed conformation syntaxin (Fig. 2*A*) (40), we expected cpd5 to displace C1aB more effectively than it displaced munc18. To confirm this prediction, we first performed a peptide array binding assay, which showed that cpd5 (100 μM) significantly reduced binding between syntaxin and all the previously identified (24) Kv2.1 C1a-derived syntaxin-binding peptides (Fig. 5). Of note, inhibition was seen for all peptides containing the predicted stacking interaction between C1aB W7 and syntaxin F34, as well as C1aB L2. We also gauged the specificity of cpd5 by noting that it had a negligible effect on any of the remaining nonspecific or weak reads. To evaluate the potency of cpd5, we measured concentration-dependent inhibition of syntaxin binding to peptides 22–28, which contain the full C1aB sequence, obtaining a fitted $IC_{50}$ of 5.5 μM with a maximum effectiveness of up to ~75% binding displacement by 100 μM Cpd5 (Fig. 5, *Inset*, fitted curve of averaged data). Higher concentrations of Cpd5 could not be tested due to solubility issues.

We next performed a coimmunoprecipitation assay of syntaxin and munc18 in transfected HEK293 cells incubated in various

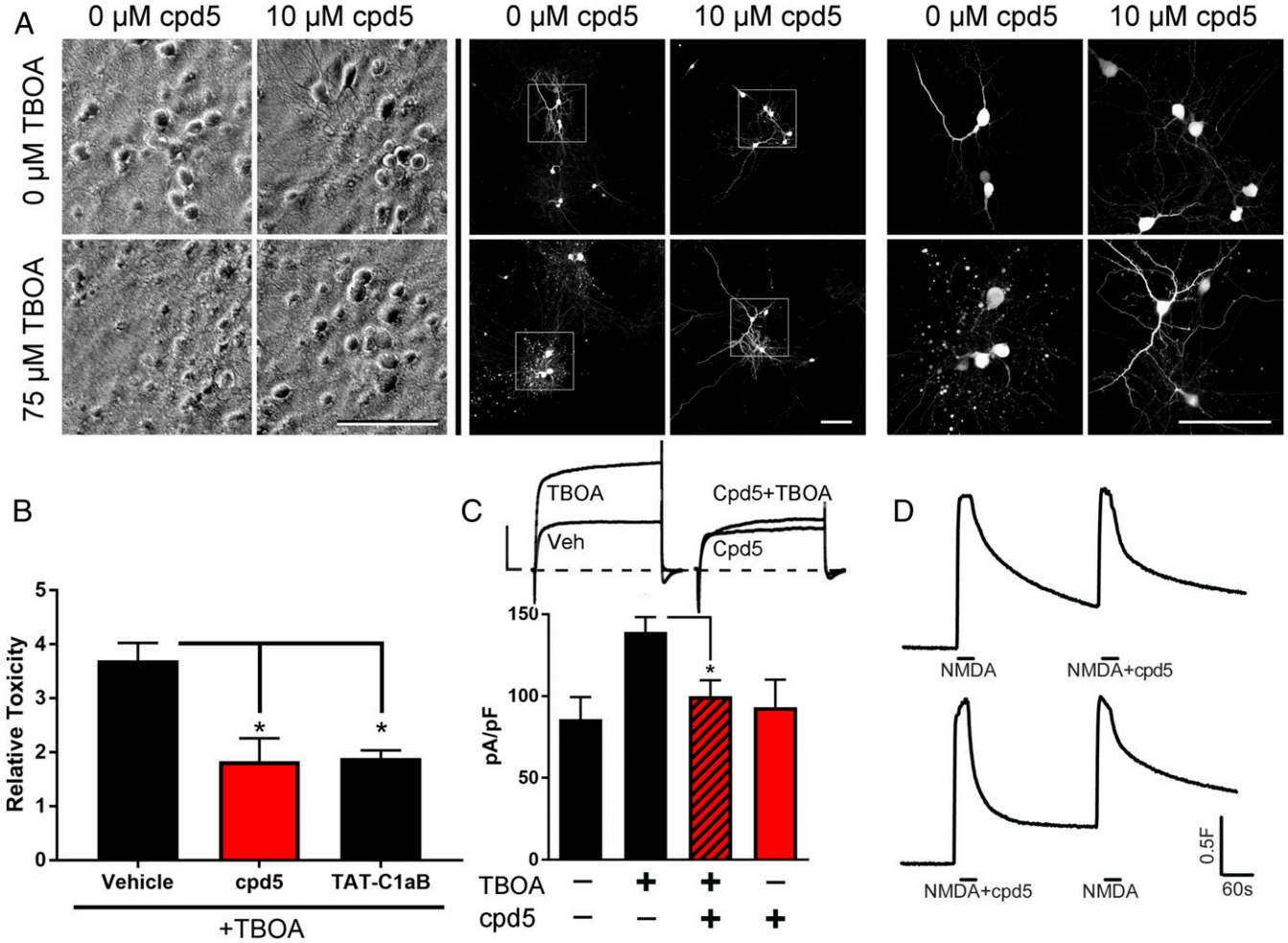


**Fig. 4.** Cpd5 suppresses death-inducing Kv2.1 current and is a neuroprotective agent. (*A*) Representative figures of the neuronal culture treated with TBOA, with and without cpd5 preincubation and coincubation. Phase-bright cells represent neurons. Subsequent panels show neurons transfected with eGFP plasmid after identical treatment as described in the text. (Scale bars: 100 μm.) (*B*) Incubation of cortical culture neurons with 10 μM cpd5 was found to be highly neuroprotective against 75 μM TBOA-induced excitotoxicity. This protective effect was comparable with that of its peptide counterpart, TAT-C1aB (1 μM). Relative toxicity, vehicle vs. cpd5 vs. TAT-C1aB (mean ± SEM): 3.70 ± 0.33 vs. 1.84 ± 0.42 vs. 1.89 ± 0.15. $*P < 0.05$; Kruskal–Wallis nonparametric ANOVA. $n = 3$–8. Relative toxicity is defined as $LDH_{TBOA+cpd5}/LDH_{cpd5}$. (*C*) Representative current traces (*Top*) and plots of the evoked delayed rectifier currents at +30 mV. The 50 μM TBOA-evoked increase in delayed rectifier current was significantly suppressed by the presence of 10 μM cpd5 (DMSO vs. TBOA vs. cpd5+TBOA: 85.92 ± 13.53 vs. 139.28 ± 9.05 vs. 100.12 ± 9.61 pA/pF; $*P < 0.05$, 1-way ANOVA/Dunnett test). $n = 10$–12. (Scale bar: 1,000 pA and 20 ms.) (*D*) Cpd5 (10 μM) did not inhibit NMDA-induced $Ca^{2+}$ responses in cultured cortical neurons (% control ± SEM: F-peak treated, 101.26 ± 1.47; AUC treated, 104.67 ± 1.98; $*P > 0.05$; *t* test). Responses shown are the average of 40 Fura-2–loaded cells in 2 separate coverslips. Four coverslips were used for our analysis, representing approximately 160 cells.

concentrations of cpd5. Consistent with our prediction, we found that cpd5, at both 30 and 100 μM, robustly disrupted binding between munc18 and syntaxin (*SI Appendix*, Fig. S2*A*); the specificity of the antibodies used in this experiment was also confirmed (*SI Appendix*, Fig. S2*B*). Of note, munc18 was not displaced by cpd5 at the neuroprotective concentration of 10 μM, which, as noted above, can displace C1aB-containing peptides from syntaxin. Taken together, these results demonstrate that the observed neuroprotective actions of cpd5 are likely due to inhibition of the C1a region of Kv2.1 binding to syntaxin.

**Cpd5 Does Not Alter Either Synaptic or Intrinsic Properties of Neurons.** Loss of munc18 function blocks neurotransmitter release, causing $munc18^{-/-}$ animals to suffer paralysis and rapid global neurodegeneration after birth (41, 42). Despite cpd5's overlapping syntaxin-binding site with that of munc18, we did not find it to be neurotoxic in vitro at concentrations as high as 30 μM (*SI Appendix*, Fig. S1*D*). Nonetheless, we deemed it necessary to evaluate the possibility that cpd5 has nonspecific effects on neuronal synaptic and intrinsic properties. For this purpose, we evaluated the effects of 10 μM cpd5 on the synaptic and intrinsic properties of 2 distinct populations of projection neurons in the mouse auditory cortex: the layer 2/3 corticocallosal neurons projecting to the contralateral auditory cortex and the layer 5B corticocollicular neurons projecting to the ipsilateral inferior colliculus (43, 44). Along with being guided by anatomic landmarks such as the rhinal fissure and the hippocampal anatomy to locate the auditory cortex, we injected green retrograde fluorospheres in the contralateral cortex and red retrograde fluorospheres in the ipsilateral inferior colliculus to label the layer 2/3 corticocallosal and layer 5B corticocollicular neuronal populations, respectively (Fig. 6*A*, *Left*). We previously confirmed that retrogradely labeled layer 2/3 corticocallosal and layer 5B corticocollicular neurons in this manner consistently overlay the functionally localized auditory cortex (43, 44). Local stimulation to layer 2/3 was used to evoke excitatory postsynaptic currents (EPSCs) in retrogradely labeled layer 2/3

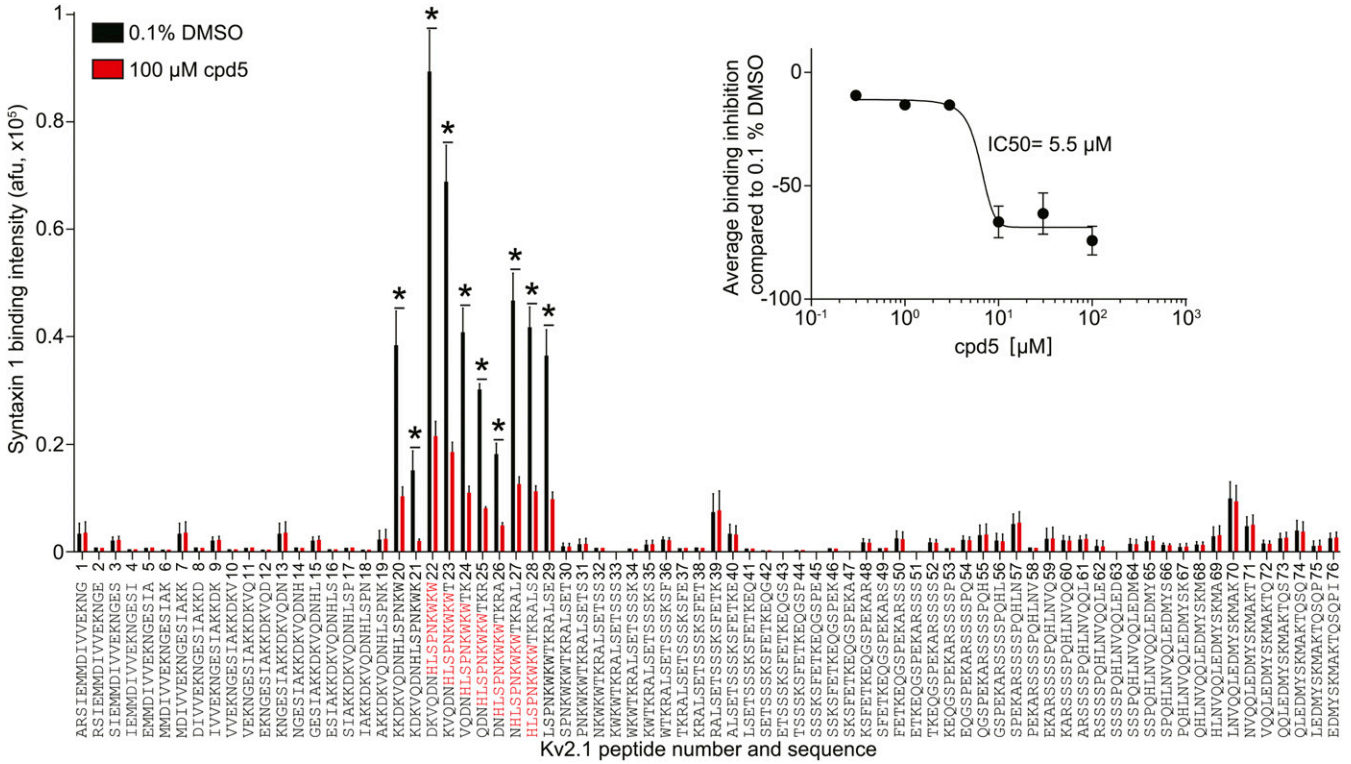


**Fig. 5.** Cpd5 competitively binds syntaxin against C1aB-containing Kv2.1 peptides. Shown are results of a peptide array binding assay of the proximal Kv2.1 C terminus (C1a) region using 15-aa segments spanning residues Kv2.1 451–540, in overlapping 1-aa steps. The bar graph summarizes ($n = 4$) of syntaxin binding intensity in the presence of 100 μM cpd5 or 0.1% DMSO as vehicle control. The C1a binding sequence is highlighted in red. *$P < 0.05$, nonparametric Mann–Whitney *U* test for each peptide. (*Inset*) Average concentration-dependent effect of cpd5 on syntaxin binding to peptides 22–28 (containing the full C1aB domain; $n = 4$ for each peptide) of the peptide array. The percent inhibition of syntaxin binding compared with 0.1% DMSO is plotted for various concentrations of cpd5. The fitted sigmoid curve to the pooled, averaged data is shown in red. The data were fitted in GraphPad Prism with a log (inhibitor) vs. normalized pooled response with a variable slope curve, yielding an $IC_{50}$ of 5.5 μM. Data are expressed as mean ± SEM of the indicated values.

corticocallosal neurons (Fig. 6*A*, *Right*). Application of cpd5 (10 μM) caused no significant differences in the amplitude of AMPAR-mediated EPSCs evoked in these cells (Fig. 6 *B–D*).

We next examined the effects of cpd5 (10 μM) on the intrinsic properties of labeled layer 5B corticocollicular neurons (*SI Appendix*, Fig. S3*A*). Cpd5 did not have any effect on resting membrane potential (*SI Appendix*, Fig. S3*B*), input resistance (*SI Appendix*, Fig. S3*C*), or HCN channel-mediated sag potential ($I_h$) (*SI Appendix*, Fig. S3*D*). Action potential threshold (*SI Appendix*, Fig. S3*E*), width (*SI Appendix*, Fig. S3*F*), and firing rates (*SI Appendix*, Fig. S3*G*) were also unchanged by the cpd5 treatment. These results demonstrate that cpd5 does not affect either the synaptic properties of layer 2/3 corticocallosal neurons or the intrinsic properties of layer 5B corticocollicular neurons in the mouse auditory cortex, consistent with the fact that the drug does not disrupt munc18–syntaxin binding at neuroprotective concentrations.

## Discussion

The interaction between the intrinsically disordered proximal C terminus of the delayed rectifier Kv2.1 (C1a) and the SNARE protein syntaxin was first characterized nearly 15 y ago by Gaisano, Lotan, and coworkers (20–22). Recent work in our laboratory narrowed down the involved Kv2.1 C1a region to 50 amino acids (23) and then to the 9-aa sequence termed C1aB (24). Preventing the interaction between Kv2.1 and syntaxin by either overexpressing C1a or using the cell-permeant TAT-C1aB peptide are effective neuroprotective strategies in both in vitro and in vivo models of acute neuronal injury (23, 24). Here we report the discovery of a first-in-class neuroprotective small molecule inhibitor (cpd5) of the protein–protein interaction between syntaxin and Kv2.1. Using molecular dynamics simulations of intrinsically disordered peptides containing the Kv2.1 syntaxin-binding sequence C1aB (HLSPNKW$_7$KW) and docking, we predicted the aromatic residue W7 to be a critical binding motif to syntaxin (Fig. 1). This prediction was validated by alanine scanning of individual C1aB residues and competitive binding assays of C1a-derived peptides that demonstrated inhibition of only those peptides containing W7 (Figs. 1*D* and 5). Furthermore, we predicted C1aB binding on the rim of the munc18 interactions with syntaxin (Fig. 2 *A* and *B*), suggesting that munc18 should form a much tighter complex with the closed conformation of syntaxin than C1a.

Most importantly, we demonstrate Kv2.1–syntaxin binding as a highly promising target for eliciting neuroprotection that does not appear to have any detrimental effects in the neuronal cell types examined. Notably, cpd5 at 10 μM is neuroprotective, effectively displacing Kv2.1 C1aB peptides from syntaxin without affecting the binding of munc18 and syntaxin, which we show occurs only at much higher concentrations (*SI Appendix*, Fig. S2*A*). Indeed, the mechanism of action predicted for cpd5 shows that besides the aromatic interaction with syntaxin F34, cpd5 also competes for direct intermolecular hydrogen bonds and nonpolar contacts formed by C1aB with syntaxin, whereas only the water-mediated interactions are significantly disrupted in the munc18–syntaxin binding (Figs. 2 *C* and *D* and 3*A*). Furthermore, the loss of the entire syntaxin N-terminal Habc globular domain, which includes the F34 residue, does not impede vesicle fusion induced by munc18 (45), indicating that exogenous competition at

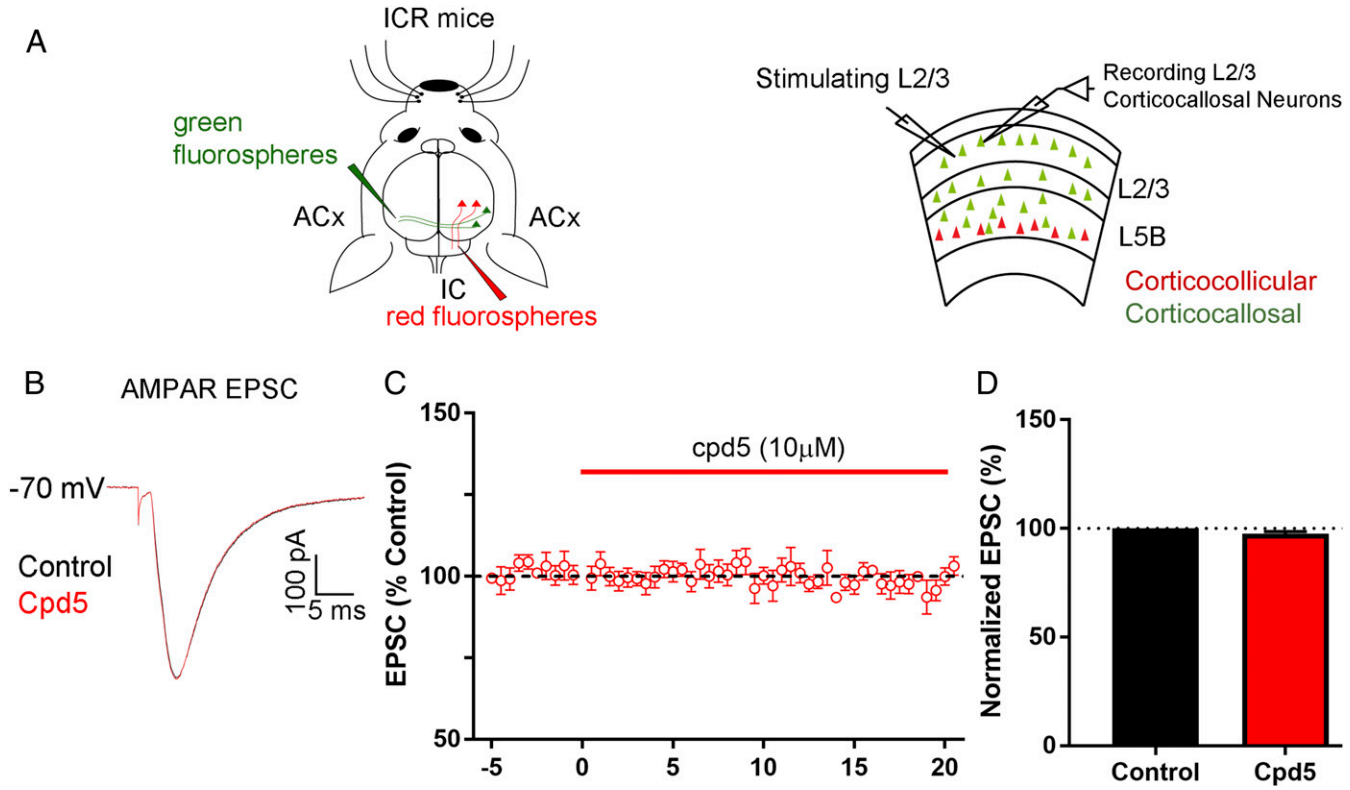


**Fig. 6.** Cpd5 (10 μM) does not affect evoked AMPAR EPSCs in layer 2/3 corticocallosal neurons in the mouse auditory cortex. (*A*, *Left*) Schematic of stereotaxic injections for labeling of corticocollicular and corticocallosal neurons with different fluorospheres to identify select neurons in the auditory cortex for acute slice electrophysiology. (*A*, *Right*) Schematic illustrating the slice electrophysiology experiment involving electrical stimulation of auditory cortex layer 2/3 while recording from adjacent labeled corticocallosal neurons. (*B*) Representative traces of a layer 2/3 corticocallosal neuron AMPAR EPSCs evoked by electrical stimulation of adjacent layer 2/3 sites during incubation in control (black) and in 10 μM cpd5 (red). (*C*) Time course of the average amplitude of AMPAR EPSCs before and after cpd5 treatment. (*D*) Average effect of cpd5 (red) on layer 2/3 corticocallosal neuron AMPAR EPSC amplitudes, normalized to control (control vs. cpd5: 97.6 ± 0.9%; $P = 0.153$, paired $t$ test). $n = 4$ cells from 4 mice.

the F34-binding site is not immediately deleterious to SNARE functions.

We did not observe the suppression of basal Kv2.1 current when targeting syntaxin. Cpd5 neither suppressed Kv2.1 current below its control levels nor increased cortical neuron excitability, consistent with our previous observations with C1a and TAT-C1aB (23, 24). This suggests distinct trafficking mechanisms between basal and death-promoting Kv2.1 channel populations. The death-promoting Kv2.1 population has been shown to be inserted de novo after lethal insults (19) and to require the existence of nonconducting Kv2.1 surface clusters that act as general protein trafficking hubs when in contact with the endoplasmic reticulum (37, 46). On the other hand, the basal Kv2.1 population does not appear to require interaction with syntaxin, as botulinum neurotoxin-mediated loss of syntaxin and SNAP-25 function only suppresses expression of the prodeath Kv2.1 currents (19). These findings strongly support the idea that basal Kv2.1 maintenance is largely syntaxin-independent and is unaffected by our neuroprotective strategy of targeting a putatively dedicated cell death pathway. The fact that Kv2.1 can be selectively transported for distinct functions was recently reinforced by a study showing that phosphoregulation of a Kv2.1 target sequence motif (amino acids 720–745) can lead to Golgi-independent trafficking of the channel to the axon initial segment (47). In the same vein, we propose that injury-dependent phosphorylation of Kv2.1 Y124 and S800 (15) drives prodeath trafficking of Kv2.1 to the membrane via the syntaxin-dependent process described here.

Kv2.1 serves several nonconducting functions through its large cytosolic domains. Most prominently, Kv2.1 directly interacts with members of the SNARE complex, SNAP-25 and VAMP2 (48, 49), in addition to syntaxin, to facilitate exocytosis and vesicle fusion in several cell types. In neuroendocrine cells, the Kv2.1–syntaxin interaction has been shown to facilitate exocytosis of dense core vesicles independent of Kv2.1's ion channel functions (21). In pancreatic β cells, the Kv2.1–syntaxin interaction modulates the release of insulin. Clustered Kv2.1 domains in secretory β cells are known to facilitate insulin granule release through the selective binding of Kv2.1 C1a (amino acids 411–522) and C1b (amino acids 523–621) to syntaxin 1A and syntaxin 3, respectively, eliciting the secretion of distinct granule populations (50, 51). Interestingly, syntaxin 3 has a significantly reduced affinity to C1a. The aligned amino acid sequences of syntaxin 1A and syntaxin 3 reveal a number of differences in the immediate residues near the central phenylalanine identified in this study (aligning syntaxin 1A's F34 to syntaxin 3's F36; UniProt alignment: Q16623 STX1A_HUMAN, Q13277 STX3_HUMAN). Specifically, in syntaxin 1A, the amino acids glutamic acid-glutamine-valine (EQV) follow phenylalanine, while in syntaxin 3, serine-glutamic acid-isoleucine (SEI) follow phenylalanine. More studies are needed to evaluate how these amino acid sequence distinctions lead to differences in binding preference. Recently, Kv2.1 was found to associate with the endoplasmic reticulum proteins VAPA and VAPB to form distinct channel clusters at contact points between the plasma membrane and the endoplasmic reticulum (52, 53). These clusters have been shown to be necessary for trafficking of the death-promoting population of Kv2.1 (36), suggesting that the interaction between Kv2.1 and the VAP proteins may be involved in cell death processes.

With the discovery of cpd5 as a first-in-class neuroprotective agent, we demonstrate a translational workflow that uses structural modeling to guide the resolution of protein–protein interactions involving poorly characterized disordered domains, leading to both mechanistic insights and identification of an effective drug. To this end, the approach of temporarily disrupting a protein–protein interaction for neuroprotection is a recently proven successful translational venture, as is seen with the TAT-NR2B9c peptide, a current phase III treatment for acute ischemic stroke that ameliorates excitotoxicity by displacing NMDA receptor function from nitric oxide production (54). While we have shown that disrupting the Kv2.1–syntaxin interaction is also efficacious in a mouse model of acute ischemic stroke (24), there is an increasing evidence of Kv2.1's involvement in even broader contexts of neurodegenerative conditions, including chronic and progressive neurologic disorders (5, 55–57). This reflects the fact that oxidative stress is a major component of most neurodegenerative conditions (58) and is known to drive the Kv2.1-mediated cell death pathway (14). As such, cpd5 not only is a first-in-class neuroprotective molecule, but also represents an important step in realizing the therapeutic potential of targeting Kv2.1 in neurodegenerative disorders.

## Materials and Methods

**Molecular Dynamics Modeling.** All initial structures of the 9-mer Kv2.1-derived peptides were built using PyMOL. The molecular dynamics simulations of Kv2.1-derived peptides were run using pmemd.cuda from AMBER14 using the AMBER ff12SB force field. Detailed parameters of the docking simulation are provided in *SI Appendix*.

**Virtual Screening Using ZINCPharmer.** The structure of the syntaxin was obtained from PDB ID code 4JEH. Several pharmacophore models were built based on the munc18–syntaxin interactions using ZINCPharmer. These structures were then submitted to SMINA for structural minimization, and 6 compounds were chosen for further experimental testing. All compounds were purchased from MolPort. Selection criteria and docking perimeters are provided in *SI Appendix*.

**Cortical Cultures.** All animal protocols described here were approved by the Institutional Animal Care and Use Committee of the University of Pittsburgh School of Medicine. Cortical culture experiments (TBOA LDH assay, patch clamp electrophysiology) were done using cortical neurons prepared from embryonic day 16–17 rats of either sex. In brief, cortices were dissociated with trypsin and plated in 6-well plates at 670,000 cells per well on poly-L-ornithine glass coverslips. Nonneuronal cell proliferation was inhibited with 1–2 μM cytosine arabinoside at 15 d in vitro (DIV). Coverslips were moved to 24-well plates for treatment. All cortical culture experiments shown here were performed on 18–25 DIV cultures.

**Peptide Spot Array and Binding Assay.** Protein-binding affinity assays were performed using peptide spot arrays (15 mer) spanning the proximal C terminus residues 451–540 of rat Kv2.1. Nitrocellulose membranes were blocked for 1 h at room temperature (RT) with gentle shaking in TBST (Tris-buffered saline, 0.1% Tween 20) containing 5% (wt/vol) nonfat dry milk and then incubated with enriched STX1A protein containing the indicated concentrations of cpd5 for 1 h at RT with gentle shaking. Next, the membrane was incubated in primary antibody for syntaxin 1A (EMD Millipore; catalog no. AB5820-50UL, RRID: AB_2216165) for 2 h at RT with gentle shaking, followed by washing with TBST. Finally, the membrane was incubated in secondary antibody (goat anti-rabbit DyLight 800, catalog no. 355571; Thermo Fisher Scientific) for 45 min, washed 3 times for 5 min each in TBST, and visualized by infrared fluorescence (Li-Cor). Similar procedures were followed for the alanine scan study with 9-mers.

**Slice Electrophysiology.** Slice electrophysiology experiments were performed in mice at least 2 d after fluorosphere injections. Coronal slices (300 μm) containing the auditory cortex were prepared in a cutting solution at 1 °C using a vibratome (VT1200 S; Leica). Slices were stored at room temperature until the time of recording. Both slice electrophysiology experiments were carried out using a MultiClamp-700B amplifier equipped with a Digidata-1440A A/D converter and Clampex (Molecular Devices). Data were sampled at 10 kHz and Bessel-filtered at 4 kHz. Pipette capacitance was compensated for, and series resistance for recordings was <15 MΩ as measured throughout the experiments. Recordings were excluded from further analysis if the series resistance changed by >15% compared with the baseline period.

Statistical analyses were performed with GraphPad Prism software and are specified in each figure. Detailed descriptions of each experiment and of calcium measurements, confocal imaging, and coimmunoprecipitation are presented in *SI Appendix*.

**ACKNOWLEDGMENTS.** We thank Gabrielle Kosobucki for performing the Kv2.1 cluster analysis. Z.Y. thanks the China Scholarship Council and the Tsinghua University–University of Pittsburgh Joint Program for the scholarship and research opportunities. This work was supported by National Institutes of Health Grants NS043277 (to E.A.), GM097082 (to C.C), and DC007905 (to T.T.).

1. Focus on neurodegenerative disease. *Nat. Neurosci.* **21**, 1293 (2018).
2. V. K. Gribkoff, L. K. Kaczmarek, The need for new approaches in CNS drug discovery: Why drugs have failed, and what can be done to improve outcomes. *Neuropharmacology* **120**, 11–19 (2017).
3. V. N. Uversky, Intrinsically disordered proteins and their (disordered) proteomes in neurodegenerative disorders. *Front. Aging Neurosci.* **7**, 18 (2015).
4. M. Kjaergaard, B. B. Kragelund, Functions of intrinsic disorder in transmembrane proteins. *Cell. Mol. Life Sci.* **74**, 3205–3224 (2017).
5. N. H. Shah, E. Aizenman, Voltage-gated potassium channels at the crossroads of neuronal function, ischemic tolerance, and neurodegeneration. *Transl. Stroke Res.* **5**, 38–58 (2014).
6. F. M. Hughes, Jr, J. A. Cidlowski, Potassium is a critical regulator of apoptotic enzymes in vitro and in vivo. *Adv. Enzyme Regul.* **39**, 157–171 (1999).
7. S. P. Yu *et al.*, Mediation of neuronal apoptosis by enhancement of outward potassium current. *Science* **278**, 114–117 (1997).
8. S. P. Yu, Regulation and critical role of potassium homeostasis in apoptosis. *Prog. Neurobiol.* **70**, 363–386 (2003).
9. S. Pal, K. A. Hartnett, J. M. Nerbonne, E. S. Levitan, E. Aizenman, Mediation of neuronal apoptosis by Kv2.1-encoded potassium channels. *J. Neurosci.* **23**, 4798–4802 (2003).
10. K. W. Wu, P. Yang, S. S. Li, C. W. Liu, F. Y. Sun, VEGF-attenuated increase of outward delayed-rectifier potassium currents in hippocampal neurons induced by focal ischemia via PI3-K pathway. *Neuroscience* **298**, 94–101 (2015).
11. X. X. Chi, Z. C. Xu, Differential changes of potassium currents in CA1 pyramidal neurons after transient forebrain ischemia. *J. Neurophysiol.* **84**, 2834–2843 (2000).
12. P. T. Redman *et al.*, A vital role for voltage-dependent potassium channels in dopamine transporter-mediated 6-hydroxydopamine neurotoxicity. *Neuroscience* **143**, 1–6 (2006).
13. S. Jiao *et al.*, cAMP/protein kinase A signalling pathway protects against neuronal apoptosis and is associated with modulation of Kv2.1 in cerebellar granule cells. *J. Neurochem.* **100**, 979–991 (2007).
14. E. Aizenman *et al.*, Induction of neuronal apoptosis by thiol oxidation: Putative role of intracellular zinc release. *J. Neurochem.* **75**, 1878–1888 (2000).
15. P. T. Redman, K. A. Hartnett, M. A. Aras, E. S. Levitan, E. Aizenman, Regulation of apoptotic potassium currents by coordinated zinc-dependent signalling. *J. Physiol.* **587**, 4393–4404 (2009).
16. P. T. Redman *et al.*, Apoptotic surge of potassium currents is mediated by p38 phosphorylation of Kv2.1. *Proc. Natl. Acad. Sci. U.S.A.* **104**, 3568–3573 (2007).
17. K. He, M. C. McCord, K. A. Hartnett, E. Aizenman, Regulation of pro-apoptotic phosphorylation of Kv2.1 $K^+$ channels. *PLoS One* **10**, e0129498 (2015).
18. M. C. McCord, E. Aizenman, Convergent $Ca2^+$ and $Zn2^+$ signaling regulates apoptotic Kv2.1 K+ currents. *Proc. Natl. Acad. Sci. U.S.A.* **110**, 13988–13993 (2013).
19. S. K. Pal, K. Takimoto, E. Aizenman, E. S. Levitan, Apoptotic surface delivery of $K^+$ channels. *Cell Death Differ.* **13**, 661–667 (2006).
20. D. Singer-Lahat *et al.*, $K^+$ channel facilitation of exocytosis by dynamic interaction with syntaxin. *J. Neurosci.* **27**, 1651–1658 (2007).
21. D. Singer-Lahat, D. Chikvashvili, I. Lotan, Direct interaction of endogenous Kv channels with syntaxin enhances exocytosis by neuroendocrine cells. *PLoS One* **3**, e1381 (2008).
22. Y. M. Leung *et al.*, Syntaxin 1A binds to the cytoplasmic C terminus of Kv2.1 to regulate channel gating and trafficking. *J. Biol. Chem.* **278**, 17532–17538 (2003).
23. M. C. McCord *et al.*, Syntaxin-binding domain of Kv2.1 is essential for the expression of apoptotic $K^+$ currents. *J. Physiol.* **592**, 3511–3521 (2014).
24. C.-Y. Yeh *et al.*, Targeting a potassium channel/syntaxin interaction ameliorates cell death in ischemic stroke. *J. Neurosci.* **37**, 5648–5658 (2017).
25. N. A. Pabon, C. J. Camacho, Probing protein flexibility reveals a mechanism for selective promiscuity. *eLife* **6**, e22889 (2017).
26. R. F. Toonen, M. Verhage, Munc18-1 in secretion: Lonely munc joins SNARE team and takes control. *Trends Neurosci.* **30**, 564–572 (2007).
27. P. Burkhardt, D. A. Hattendorf, W. I. Weis, D. Fasshauer, Munc18a controls SNARE assembly through its interaction with the syntaxin N-peptide. *EMBO J.* **27**, 923–933 (2008).
28. J. Jiao *et al.*, Munc18-1 catalyzes neuronal SNARE assembly by templating SNARE association. *eLife* **7**, e41771 (2018).
29. D. R. Koes, M. P. Baumgartner, C. J. Camacho, Lessons learned in empirical scoring with smina from the CSAR 2011 benchmarking exercise. *J. Chem. Inf. Model.* **53**, 1893–1904 (2013).
30. D. R. Koes, C. J. Camacho, ZINCPharmer: Pharmacophore search of the ZINC database. *Nucleic Acids Res.* **40**, W409-14 (2012).

31. J. J. Irwin, B. K. Shoichet, ZINC—A free database of commercially available compounds for virtual screening. *J. Chem. Inf. Model.* **45**, 177–182 (2005).
32. Z. Ye, M. P. Baumgartner, B. M. Wingert, C. J. Camacho, Optimal strategies for virtual screening of induced-fit and flexible target in the 2015 D3R grand challenge. *J. Comput. Aided Mol. Des.* **30**, 695–706 (2016).
33. M. Aras, K. Hartnett, E. Aizenman, Assessment of cell viability in primary neuronal cultures. *Curr. Protoc. Neurosci.* **44**, 7.18.1–7.18.15 (2008).
34. K. Shimamoto *et al*., DL-threo-β-benzyloxyaspartate, a potent blocker of excitatory amino acid transporters. *Mol. Pharmacol.* **53**, 195–201 (1998).
35. J. A. Justice *et al*., Molecular neuroprotection induced by zinc-dependent expression of hepatitis C-derived protein NS5A targeting Kv2.1 potassium channels. *J. Pharmacol. Exp. Ther.* **367**, 348–355 (2018).
36. J. A. Justice *et al*., Disruption of $K_V$2.1 somato-dendritic clusters prevents the apoptogenic increase of potassium currents. *Neuroscience* **354**, 158–167 (2017).
37. R. Blitzblau, S. Gupta, S. Djali, M. B. Robinson, P. A. Rosenberg, The glutamate transport inhibitor L-trans-pyrrolidine-2,4-dicarboxylate indirectly evokes NMDA receptor-mediated neurotoxicity in rat cortical cultures. *Eur. J. Neurosci.* **8**, 1840–1852 (1996).
38. R. Sattler, M. Tymianski, Molecular mechanisms of glutamate receptor-mediated excitotoxic neuronal cell death. *Mol. Neurobiol.* **24**, 107–129 (2001).
39. D. W. Choi, Ionic dependence of glutamate neurotoxicity. *J. Neurosci.* **7**, 369–379 (1987).
40. K. M. Misura, R. H. Scheller, W. I. Weis, Three-dimensional structure of the neuronal-Sec1-syntaxin 1a complex. *Nature* **404**, 355–362 (2000).
41. M. Verhage *et al*., Synaptic assembly of the brain in the absence of neurotransmitter secretion. *Science* **287**, 864–869 (2000).
42. R. M. Weimer *et al*., Defects in synaptic vesicle docking in unc-18 mutants. *Nat. Neurosci.* **6**, 1023–1030 (2003).
43. A. Joshi *et al*., Cell-specific activity-dependent fractionation of layer 2/3→5B excitatory signaling in mouse auditory cortex. *J. Neurosci.* **35**, 3112–3123 (2015).
44. A. Joshi, B. I. Kalappa, C. T. Anderson, T. Tzounopoulos, Cell-specific cholinergic modulation of excitability of layer 5B principal neurons in mouse auditory cortex. *J. Neurosci.* **36**, 8487–8499 (2016).
45. J. Shen, S. S. Rathore, L. Khandan, J. E. Rothman, SNARE bundle and syntaxin N-peptide constitute a minimal complement for Munc18-1 activation of membrane fusion. *J. Cell Biol.* **190**, 55–63 (2010).
46. P. D. Fox *et al*., Induction of stable ER-plasma-membrane junctions by Kv2.1 potassium channels. *J. Cell Sci.* **128**, 2096–2105 (2015).
47. C. S. Jensen *et al*., Trafficking of Kv2.1 channels to the axon initial segment by a novel nonconventional secretory pathway. *J. Neurosci.* **37**, 11523–11536 (2017).
48. P. E. MacDonald *et al*., Synaptosome-associated protein of 25 kilodaltons modulates Kv2.1 voltage-dependent K(+) channels in neuroendocrine islet β-cells through an interaction with the channel N terminus. *Mol. Endocrinol.* **16**, 2452–2461 (2002).
49. A. Lvov, D. Chikvashvili, I. Michaelevski, I. Lotan, VAMP2 interacts directly with the N terminus of Kv2.1 to enhance channel inactivation. *Pflugers Arch.* **456**, 1121–1136 (2008).
50. D. Greitzer-Antes *et al*., Kv2.1 clusters on β cell plasma membrane act as reservoirs that replenish pools of newcomer insulin granules through their interaction with syntaxin-3. *J. Biol. Chem.* **293**, 6893–6904 (2018).
51. D. Zhu *et al*., Syntaxin-3 regulates newcomer insulin granule exocytosis and compound fusion in pancreatic beta cells. *Diabetologia* **56**, 359–369 (2013).
52. B. Johnson *et al*., Kv2 potassium channels form endoplasmic reticulum/plasma membrane junctions via interaction with VAPA and VAPB. *Proc. Natl. Acad. Sci. U.S.A.* **115**, E7331–E7340 (2018).
53. M. Kirmiz, N. C. Vierra, S. Palacio, J. S. Trimmer, Identification of VAPA and VAPB as Kv2 channel-interacting proteins defining endoplasmic reticulum–plasma membrane junctions in mammalian brain neurons. *J. Neurosci.* **38**, 7562–7584 (2018).
54. B. Ballarin, M. Tymianski, Discovery and development of NA-1 for the treatment of acute ischemic stroke. *Acta Pharmacol. Sin.* **39**, 661–668 (2018).
55. M. C. McCord, E. Aizenman, The role of intracellular zinc release in aging, oxidative stress, and Alzheimer's disease. *Front. Aging Neurosci.* **6**, 77 (2014).
56. Y. Wei, M. R. Shin, F. Sesti, Oxidation of KCNB1 channels in the human brain and in mouse model of Alzheimer's disease. *Cell Death Dis.* **9**, 820 (2018).
57. R. Y. Chao, C. H. Cheng, S. N. Wu, P. C. Chen, Defective trafficking of Kv2.1 channels in MPTP-induced nigrostriatal degeneration. *J. Neurochem.* **144**, 483–497 (2018).
58. Z. Liu, T. Zhou, A. C. Ziegler, P. Dimitrion, L. Zuo, Oxidative stress in neurodegenerative diseases: From molecular mechanisms to clinical applications. *Oxid. Med. Cell. Longev.* **2017**, 2525967 (2017).